Chinese Chemical Letters 31 (2020) 2063–2066

Contents lists available at ScienceDirect

Chinese Chemical Letters

journal homepage: www.elsevier.com/locate/cclet

Communication

Preparation and formaldehyde sensitive properties of N-GQDs/SnO_2 nanocomposite

Zhenlu Chen, Ding Wang, Xianying Wang*, Junhe Yang

School of Material Science & Engineering, University of Shanghai for Science and Technology, Shanghai 200093, China

ARTICLE INFO

Article history:
Received 12 October 2019
Received in revised form 20 November 2019
Accepted 26 November 2019
Available online 27 November 2019

Keywords:
Formaldehyde gas sensor
Graphene quantum dots
Nitrogen-doped graphene quantum dots
Nanocomposites
Nanosheets

ABSTRACT

Graphene quantum dots (GQDs) have both the properties of graphene and semiconductor quantum dots, and exhibit stronger quantum confinement effect and boundary effect than graphene. In addition, the band gap of GQDs will transform to non-zero from 0 eV of graphene by surface functionalization, which can be dispersed in common solvents and compounded with solid materials. In this work, the SnO_2 nanosheets were prepared by hydrothermal method. As the sensitizer, nitrogen-doped graphene quantum dots (N-GQDs) were prepared and composited with SnO_2 nanosheets. Sensing performance of pristine SnO_2 and N-GQDs/SnO_2 were investigated with HCHO as the target gas. The response (R_a/R_g) of 0.1% N-GQDs/SnO_2 was 256 for 100 ppm HCHO at 60 °C, which was about 2.2 times higher than pristine SnO_2 nanosheet. In addition, the material also had excellent selectivity and low operation temperature. The high sensitivity of N-GQDs/SnO_2 was attributed to the increase of active sites on materials surface and the electrical regulation of N-GQDs. This research is helpful to develop new HCHO gas sensor and expand the application field of GQDs.

As an important chemical material, HCHO is widely used in home decoration, chemical industry, wood industry, textile industry and so on [1]. HCHO vapor may cause eye, nose or throat irritant reaction, which leads to sneezing, coughing, nausea, or even carcinogenesis [2]. Hence, it is imperative for developing HCHO gas sensors to protect people's health [3]. Metal oxide semiconductors (MOS), such as SnO_2, WO_3, TiO_2 and ZnO, have been widely used in semiconductor gas sensors due to their high sensitivity and low cost [4]. However, for HCHO gas detection, the poor selectivity and instability due to high operating temperature hinder practical application of MOS sensors [5]. The structural regulation and composite sensitization have been used to improve their sensitive properties. For example, 2D SnO_2 nanosheets with a large specific surface have good HCHO gas-sensing property due to abundant active sites on the surface [6]. Furthermore, many studies proved that carbon materials such as graphene oxide (GO), reduced graphene oxide (rGO), carbon nanotubes (CNTs) and g-C_3N_4 as sensitizers can effectively improve the sensitive property or decrease the operating temperature of MOS gas sensors [7–12].

GQDs with single or few-layer graphene have been considered as a potential material by the unique size-dependent of energy band gap, photoluminescence and electron transport ability. Because of these unique properties, GQDs have attracted an increasing interest in the application of energy conversion [13], anticorrosion [14], photodetectors [15], photocatalyst [16], and sensors [17–19]. However, it is still the early stage of development for applications in gas sensors [20,21] because of the drawbacks such as low sensitivity and slow response. Element-doping of GQDs may be a facile solution. GQDs can be easily doped with other elements to modulate their semiconducting properties [22,23]. Many studies indicated that nitrogen dopants could drastically alter the electronic characteristics of GQDs and offer more active sites, thus producing new phenomena and unexpected properties [24].

In this work, SnO_2 nanosheets, GQDs and N-GQDs were prepared by hydrothermal method, respectively. Then, the N-GQDs/SnO_2 nanocomposite was prepared by impregnation method. The microstructure, morphology and chemical state of N-GQDs/SnO_2 samples were investigated by X-ray diffraction analysis (XRD), transmission electron microscopy (TEM), Raman spectrum and so on. In addition, the operating temperature, response, selectivity and repeatability of sensors were studied by using a gas sensor evaluation system. The test results indicated that the sensing performance of SnO_2 to HCHO was enhanced by addition of N-GQDs. Finally, the gas-sensing mechanism of the N-GQDs/SnO_2 nanocomposite was discussed.

* Corresponding author.
E-mail address: xianyingwang@usst.edu.cn (X. Wang).

https://doi.org/10.1016/j.cclet.2019.11.043
1001-8417/

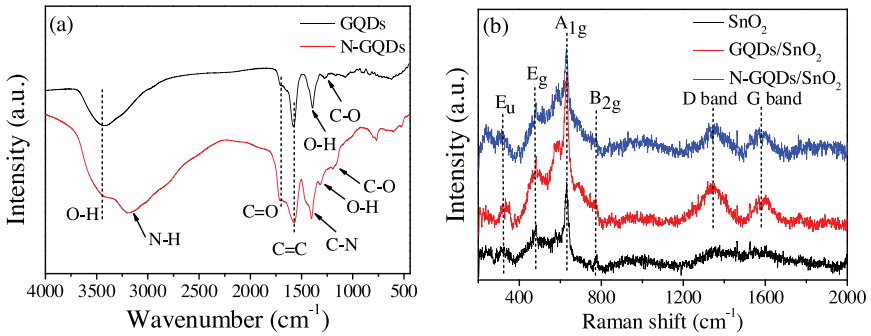

Fig. 1. (a) FTIR spectra of GQDs and N-GQDs; (b) Raman spectra of pristine SnO_2, GQDs/SnO_2 and N-GQDs/SnO_2.

To synthesis the SnO_2 nanosheets [25], 0.5 g polyvinyl pyrrolidone (PVP) was firstly added into 40 mL mixed solution of ethanol and water (1:1) under vigorous. Then 10 mmol $Na_3C_6H_5O_7{\cdot}2H_2O$ and 5 mmol $SnCl_2{\cdot}2H_2O$ were successively added into the mixed solution under vigorous stirring. After stirring, the resultant solution was loaded into a 50 mL Teflon-lined stainless autoclave, which was sealed and heated to 180 °C for 12 h. The obtained product was washed by deionized water and ethanol sequentially, and finally annealed at 500 °C for 2 h. N-GQDs were synthesized through a hydrothermal route [26]. GQDs were synthesized for the same method except using sodium hydroxide instead of urea. N-GQDs/SnO_2 composites were prepared as following: N-GQDs powders were dispersed into deionized water and sonicated for 2 h to obtain uniform solution. A certain amount of N-GQDs solution was impregnated into SnO_2 nanosheets under ultrasonic. The nanocomposite was obtained after drying at 60 °C.

FTIR spectra of GQDs and N-GQDs are shown in Fig. 1a. Besides the two peaks including O—H bending vibration at 1390 cm^{-1} and C–O vibration at 1260 cm^{-1} for both samples [27], the peaks for N-GQDs also includes N—H vibration at ~3200 cm^{-1} [26] and C–N vibration at 1396 cm^{-1} [28]. The absorption peaks for both GQDs at ~3400 cm^{-1} [26], 1718 cm^{-1} [12] and 1561 cm^{-1} [28] could be ascribed to the O—H stretching, C=O and C=C vibrations, respectively. FTIR spectra revealed that there were abundant organic functional groups on the surface of GQDs. Fig. 1b showed the Raman spectra of SnO_2, GQDs/SnO_2 and N-GQDs/SnO_2. The Raman shift at around 323 cm^{-1}, 479 cm^{-1}, 627 cm^{-1} and 775 cm^{-1} were assigned to the E_u, E_g, A_{1g} and B_{2g} vibrational modes of SnO_2, respectively [29]. In addition, the D and G bands were also found for GQDs/SnO_2 and N-GQDs/SnO_2 at 1340 cm^{-1} and 1575 cm^{-1}, respectively [30], which indicated the existence of graphene structure in both nanocomposites.

Figs. 2a–d showed TEM images of GQDs and N-GQDs, respectively. The lateral size of GQDs and N-GQDs was both in the range of 3–7 nm. The HRTEM images of GQDs and N-GQDs indicated that the interplanar crystal spacing of both samples were 0.21 nm which assigned to the (100) plane of graphene [26]. The morphology of SnO_2 nanosheets was characterized by SEM. As shown in Fig. 2e, the sample displayed flower-like structure which was assembled by nanosheets. In addition, the nanosheets exhibited smooth surface with the size about 200–400 nm. Fig. 2f showed HRTEM images of pristine SnO_2. The thickness of SnO_2 nanosheets was about 5–8 nm, and the interplanar crystal spacing of nanosheets was measured as 0.33 nm and 0.26 nm corresponding to the (110) and (101) planes of tetragonal SnO_2, respectively [7]. Fig. 2g showed TEM image of N-GQDs/SnO_2. N-GQDs were marked by red circles. Fig. 2h showed HRTEM images of N-GQDs/SnO_2. N-GQDs were marked by red circles, and the interplanar crystal spacing of N-GQDs was measured as 0.21 nm corresponding to Fig. 2d. The interplanar crystal spacing of SnO_2 nanosheets was measured as 0.33 nm and 0.26 nm corresponding to Fig. 2f.

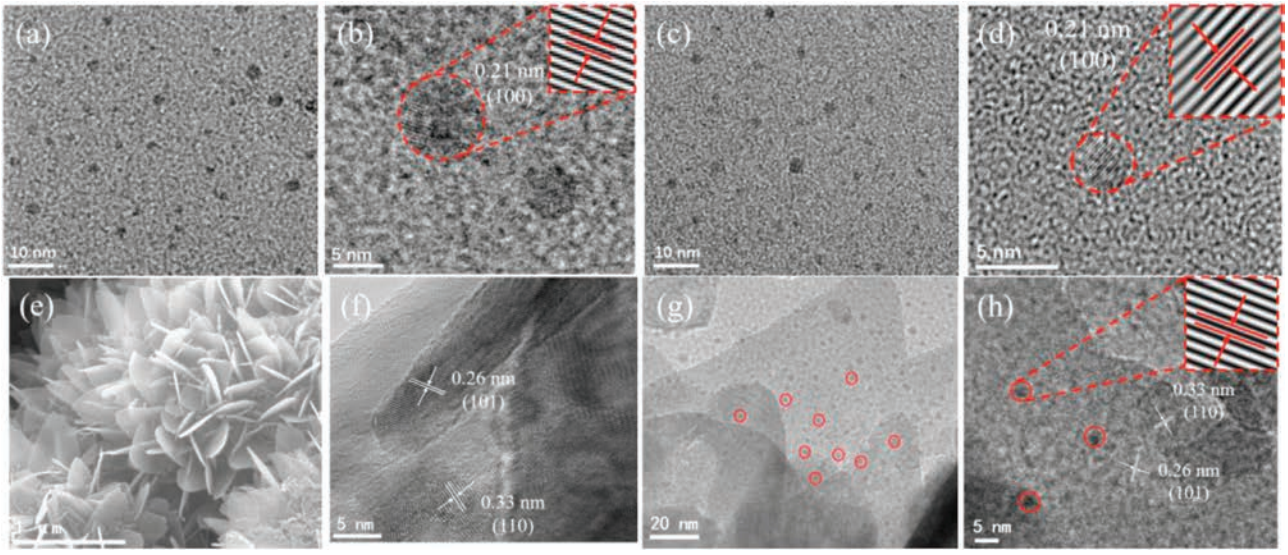

Fig. 2. (a) TEM image of GQDs. (b) HRTEM image of GQDs. (c) TEM image of N-GQDs. (d) HRTEM image of N-GQDs. (e) SEM image of SnO_2 nanosheets. (f) HRTEM image of SnO_2 nanosheets. (g) TEM image of N-GQDs/SnO_2. (h) HRTEM of N-GQDs/SnO_2. The insets are the autocorrelated HRTEM lattice images recorded from the corresponding selected areas.

XPS was used to study the elemental composition and the chemical states of the samples. Fig. S1a (Supporting information) showed the C 1s spectra of GQDs and N-GQDs. The C 1s spectra of GQDs could be deconvoluted into three peaks including a C=C peak with a binding energy of 284.8 eV [27], a C–O peak with a binding energy of 286.4 eV and an O—C=O peak with a binding energy of 288.3 eV [31]. The C 1s spectra of N-GQDs could be deconvoluted into four peaks including a C=C peak with a binding energy of 284.7 eV [27], a C–O peak with a binding energy of 286.6 eV, an O—C=O peak with a binding energy of 288.4 eV and a C–N/C=N peak with a binding energy of 285.4 eV [26,31]. These signals suggested that there were various oxygen containing functional groups on the surface of GQDs. Fig. S1b (Supporting information) showed the high-resolution spectrum of N 1s for N-GQDs (Support information). It could be deconvoluted into two peaks which included a NH_2 peak with a binding energy of 399.9 eV and a N—C peak with a binding energy of 401.4 eV [31]. It revealed that nitrogenous functional groups also existed on the surface of N-GQDs. Fig. S1c (Supporting information) showed the C 1s spectrum of GQDs/SnO_2 and N-GQDs/SnO_2. The C 1s spectrum of GQDs/SnO_2 could be differentiated into three peaks centered at 284.8 eV, 286.1 eV and 289.2 eV corresponding to C=C bonds, C–O bonds and O—C=O bonds, respectively. The C 1s spectrum of N-GQDs/SnO_2 could be differentiated into four peaks with centers at 284.8 eV, 285.6 eV, 286.4 eV and 289.2 eV corresponding to C=C bonds, C–N/C=N bonds, C–O bonds and O—C = O bonds, respectively [26,27,31]. The N 1s spectrum of N-GQDs/SnO_2 shown in Fig. S1d (Supporting information) could be differentiated into two peaks centered at 399.8 eV and 402 eV, which were assigned to NH_2 groups and N—C bonds, respectively [31].

The HCHO sensing properties of sensitive materials were studied. The optimal operation temperature was obtained by testing these sensors from 20 °C to 100 °C. As shown in Fig. 3a, all optimum temperatures of sensors toward HCHO were 60 °C. The response value (R_a/R_g) of pristine SnO_2, GQDs/SnO_2 and N-GQDs/SnO_2 were about 115, 153 and 256 at 60 °C, respectively. Obviously, when SnO_2 was composited with N-GQDs, the HCHO gas sensing properties were improved more dramatically than GQDs. As shown in Fig. S2 (Supporting information), 0.1% was confirmed as the best N-GQDs amount in N-GQDs/SnO_2. As shown in Fig. S1, nitrogen dopants introduced abundant N-containing species, especially amino groups on the edges of N-GQDs, which provided more active adsorption sites for gas molecules [24]. Besides, nitrogen dopants also drastically altered the electron delocalization and charge-carrier density of N-GQDs [26]. Furthermore, the selectivity, stability and response/recovery of pristine SnO_2, GQDs/SnO_2 and N-GQDs/SnO_2 gas sensors were also researched. As shown in Fig. 3b, all sensors showed high response to HCHO, while they had relatively low response to other typical interfering gas, which indicated their good selectivity to HCHO. As shown in Fig. 3c, the cycling stability of N-GQDs/SnO_2 was tested for 100 ppm HCHO in the 5 cycles. The response of N-GQDs/SnO_2 almost remained the same magnitude in the 5 cycles, and the curve could recover the original state, which presented good stability and repeatability.

Figs. 3d and e showed typical response and recovery curves with the concentration of HCHO increasing from 0.1 ppm to 100 ppm at 60 °C. The response of N-GQDs/SnO_2 was higher than that of pristine SnO_2 and GQDs/SnO_2 in all concentration range. Therefore, the HCHO gas sensor of N-GQDs/SnO_2 can be used in ppm or sub-ppm levels detection. In addition, the correlation line between concentration of HCHO and response of sensors was fitted and shown in Fig. 3f. The response was proportional to the concentration of HCHO from 0.1 ppm to 100 ppm. As shown in Fig. 3g, the response of sensors relatively maintained the original value after twenty days, which indicated the good long-term stability of the gas sensors. The HCHO sensing properties of N-GQDs/SnO_2 are compared with other SnO_2-based gas sensors (Table S1 in Supporting information). Compared to SnO_2-based materials, N-GQDs/SnO_2 gas sensor has a relatively lower operation temperature and higher sensitivity. In brief, the gas sensor of N-GQDs/SnO_2 exhibited excellent gas sensing properties in HCHO detection.

The gas sensing activity of MOS is based on the resistance change of the semiconductor when exposed in target gas [10]. The schematic diagram of gas sensing mechanism was shown in Fig. S3 (Supporting information). When the sensors were exposed to air at an opportune operation temperature, absorbed oxygen

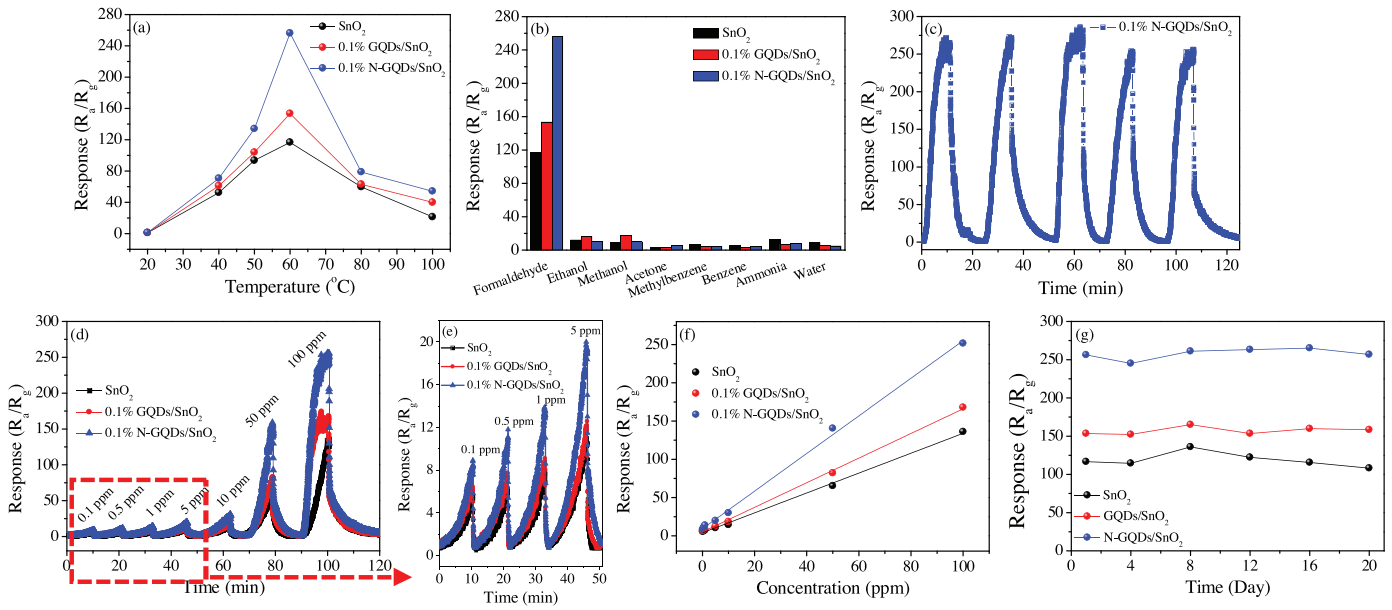

Fig. 3. (a) Response of pristine SnO_2, 0.1% GQDs/SnO_2 and 0.1% N-GQDs/SnO_2 to 100 ppm HCHO at operating temperature of 20–100 °C. (b) Response of pristine SnO_2, 0.1% GQDs/SnO_2 and 0.1% N-GQDs/SnO_2 to 100 ppm different gases at 60 °C. (c) Cycle stability of 0.1% N-GQDs/SnO_2 to 100 ppm HCHO. (d) Response/recovery curves of gas sensors to 0.1–100 ppm HCHO. (e) The response of sensors to 0.1–5 ppm HCHO. (f) The relationship between the response value and HCHO concentration. (g) Long-term stability of sensors to 100 ppm HCHO at 60 °C.

(O_2^-, O^- or O^{2-}) was formed on the surface of the materials. Meanwhile a thick electron depletion layer and a high potential barrier also appeared. It generated the increase in the resistance of the sensors. The kind of absorbed oxygen (O_2^-, O^- or O^{2-}) was determined by the operation temperature (t_{op}) [8] described by the following equations:

$$O_2\ (gas) \rightarrow O_2\ (ads) \quad (1)$$

$$O_2\ (ads) + e^- \rightarrow O_2^-\ (ads)\ (t_{op} < 100\,^\circ C) \quad (2)$$

$$O_2^-\ (ads) + e^- \rightarrow 2O^-\ (ads)\ (100\,^\circ C < t_{op} < 300\,^\circ C) \quad (3)$$

As the optimal operation temperature was confirmed at 60 °C, the redox reaction between the absorbed oxygen ions (O_2^-) and HCHO molecules could be expressed as follow [7]:

$$HCHO\ (g) + O_2^-\ (ads) \rightarrow HCOOH\ (g) + e^- \quad (4)$$

$$HCHO\ (g) + O_2^-\ (ads) \rightarrow CO_2\ (g) + H_2O\ (g) + e^- \quad (5)$$

During the reaction, the electrons were released back to their conduction band, and the injection electrons could reduce the electron depletion region and increase the conductivity of the sensor improving [5]. The high sensing performance of N-GQDs/SnO_2 was due to the 2D structure of SnO_2 nanosheets, which could enlarge the specific surface area of the material and help to improve the adsorption of HCHO molecules. Furthermore, N-GQDs could shorten the transport paths of electrons to improve the charge transfer of sensitive materials [12].

In conclusion, a high sensitivity HCHO sensor based on N-GQDs/SnO_2 nanocomposites has been successfully synthesized, which took advantage of the synergistic effect of SnO_2 nanosheets and N-GQDs. Compared with unmodified SnO_2 nanosheets, the N-GQDs/SnO_2 nanocomposite exhibited higher gas response. The unique sensing properties were attributed to the synergistic effect including the increasing active sites on the surface of nanosheets and regulating the electrical properties after modifying N-GQDs.

Declaration of competing interest

We declare that we do not have any commercial or associative interest to this work.

Acknowledgments

We greatly thank the financial supports from the National Natural Science Foundation of China (Nos. 51602197, 51771121 and 51702212), Shanghai Municipal Science and Technology Commission (Nos. 19ZR1435200, 18511110600 and 19JC1410402), Innovation Program of Shanghai Municipal Education Commission (No. 2019-01-07-00-07-E00015), Shanghai Academic/Technology Research Leader Program (No. 19XD1422900).

Appendix A. Supplementary data

Supplementary material related to this article can be found, in the online version, at doi:https://doi.org/10.1016/j.cclet.2019.11.043.

References

[1] T. Salthammer, Angew. Chem. Int. Ed. 52 (2013) 3320–3327.
[2] G.J. Li, Z.X. Cheng, Q. Xiang, et al., Sens. Actuator. B: Chem. 283 (2019) 590–601.
[3] E.M. Lee, S.Y. Gwon, Y.A. Son, S.H. Kim, Chin. Chem. Lett. 23 (2012) 484–487.
[4] Y.L. Wang, S. Tan, J. Wang, et al., Chin. Chem. Lett. 22 (2011) 603–606.
[5] X. Zhou, X. Cheng, Y. Zhu, et al., Chin. Chem. Lett. 29 (2018) 405–416.
[6] D. Wang, L. Tian, H. Li, et al., ACS Appl. Mater. Interfaces 11 (2019) 12808–12818.
[7] D. Wang, M. Zhang, Z. Chen, et al., Sens. Actuator. B: Chem. 250 (2017) 533–542.
[8] D. Wang, S. Huang, H. Li, et al., Sens. Actuator. B: Chem. 282 (2019) 961–971.
[9] H. Mu, K. Wang, S. Zhang, et al., IEEE Sens. J. 14 (2014) 2362–2368.
[10] Y. Li, D.L. Li, J.C. Liu, Chin. Chem. Lett. 26 (2015) 304–308.
[11] J. Sun, S. Bai, Y. Tian, et al., Sens. Actuator. B: Chem. 257 (2018) 29–36.
[12] Y. Zhang, J. Zhao, H. Sun, et al., Sens. Actuator. B: Chem. 266 (2018) 364–374.
[13] F. Li, L. Kou, W. Chen, et al., NPG Asia Mater. 5 (2013) e60.
[14] B.K. Jiang, A.Y. Chen, J.F. Gu, et al., Carbon 157 (2020) 537–548.
[15] Q. Zhang, J. Jie, S. Diao, et al., ACS Nano 9 (2015) 1561–1570.
[16] B. Huang, Jb. He, S.Y. Bian, et al., Chin. Chem. Lett. 29 (2018) 1698–1701.
[17] D. Wang, L. Wang, X. Dong, et al., Carbon 50 (2012) 2147–2154.
[18] L.L. Li, J. Ji, R. Fei, et al., Adv. Funct. Mater. 22 (2012) 2971–2979.
[19] Y. Zhang, C. Wu, X. Zhou, et al., Nanoscale 5 (2013) 1816–1819.
[20] L. Nguyen, P. Phan, H. Duong, et al., Sensors 13 (2013) 1754–1762.
[21] S.C. Hernandez, D. Chaudhuri, W. Chen, et al., Electroanalysis 19 (2007) 2125–2130.
[22] J.K. Wassei, K.C. Cha, V.C. Tung, et al., J. Mater. Chem. 21 (2011) 3391–3396.
[23] Y.M. Zhang, Y.T. Lin, J.L. Chen, et al., Sens. Actuator. B: Chem. 190 (2014) 171–176.
[24] Y. Li, Y. Zhao, H. Cheng, et al., J. Am. Chem. Soc. 134 (2011) 15–18.
[25] T. Li, W. Zeng, H. Long, et al., Sens. Actuator. B: Chem. 231 (2016) 120–128.
[26] H.J. Li, X. Sun, F.F. Xue, et al., ACS Sustain. Chem. Eng. 6 (2017) 1708–1716.
[27] D. Qu, M. Zheng, P. Du, et al., Nanoscale 5 (2013) 12272–12277.
[28] Y. Ma, A.Y. Chen, X.F. Xie, et al., Talanta 196 (2019) 563–571.
[29] A. Dieguez, A. Romano-Rodrıguez, A. Vila, et al., J. Appl. Phys. 90 (2001) 1550–1557.
[30] P. He, J. Sun, S. Tian, et al., Chem. Mater. 27 (2014) 218–226.
[31] X. Sun, H.J. Li, N. Ou, et al., Molecules 24 (2019) 344.